

AC Impedance Spectroscopy, Conductivity and Optical Studies of Sr doped Bismuth Ferrite Nanocomposites

Baljinder Kaur^{1,2,6}, Lakhbir Singh^{1,2,6}, V. Annapu Reddy³, Dae-Yong Jeong⁴, Navneet Dabra^{5,*},
Jasbir S. Hundal⁶

¹Department of YCoE Punjabi University Guru Kashi Campus Talwandi Sabo-151302, Punjab, India

²Research Scholar, IK Gujral Punjab Technical University Kapurthala-144001, Punjab, India

³Functional Ceramics Research Group, Korea Institute of Materials Science (KIMS),
Gyeongnam 641-831, Korea

⁴Department of Materials Science and Engineering, Inha University, Incheon-402-751, Republic of
Korea

⁵Mata Sahib Kaur Girls' College (affiliated to Punjabi University Patiala), Talwandi Sabo-151302,
Punjab, India

⁶Materials Science Laboratory, Department of Applied Physics, Giani Zail Singh Campus College of
Engineering and Technology, MRS State Technical University Bathinda-151001, Punjab, India

*E-mail: navneetdabra@gmail.com

Received: 10 January 2016 / Accepted: 11 March 2016 / Published: 1 April 2016

Effect of Sr doping on the structural, optical, dielectric, impedance properties of citrate combustion reaction route prepared $\text{Bi}_{1-x}\text{Sr}_x\text{FeO}_3$ (BSFO) nanocomposite has been investigated. The study of Fourier Transform Infrared Spectroscopy confirms the formation of perovskite structure of the Sr doped bismuth ferrite samples. SEM analysis shows decrease in grain size with increasing Sr concentration in BSFO nanocomposite. UV-visible absorption spectra in the spectral range 1.0–3.5 eV showed two doubly degenerate d–d transitions and two charge transfer transitions and optical band gap is found to decrease from 2.14 to 2.05 eV with increasing Sr concentration. Studies of frequency and temperature dependences of dielectric permittivity, impedance and electric modulus of the materials in broad frequency (20 Hz- 1 MHz) and temperature (30°C – 500°C) ranges using a complex impedance spectroscopy technique have provided interesting information on the contribution of the microstructure in these parameters. It has been observed that dielectric constant and dielectric losses decreases as the doping of Sr increased from $x=0.1$ to $x=0.3$ and attained a maximum value for BSFO ($x = 0.1$) sample. Impedance analysis indicates the presence of grain (bulk) and grain boundary resistive contributions which are found to increase with the increased Sr content. The ac conductivity of the samples is found to be frequency and temperature dependent and also vary with extent of Sr doping in BFO. Charge transport through short as well as long range conduction contributions has been indicated in different temperature regions of conductivity studies.

Keywords: Bismuth ferrite; microstructure; dielectric response; complex impedance spectroscopy

doi: 10.20964/110353

1. INTRODUCTION

Multiferroic materials are unique due to simultaneous exhibition of ferroelectric, ferroelastic, and ferromagnetic properties [1]. The coupling between their order parameters is the attracting trait of the multiferroic materials that enables manoeuvring of the magnetic and electric polarizations by electric and magnetic fields, respectively [2,3]. Amongst the multiferroic materials, BiFeO₃ (BFO) has been studied rigorously due to its multiferroic properties at room temperature (RT) [4, 5]. BFO (environment friendly material) is the only single phased perovskite multiferroic having a rhombohedrally distorted structure (space group R3c) at RT with a high ferroelectric Curie temperature and G-type antiferromagnetic Neel temperature [6, 7]. It extends a wide possibility for applications in the fabrication of multifunctional devices, such as sensors, actuators, multi-state electronic devices, photovoltaic devices, information storage, spintronics devices and so on [4].

Several Research groups have tried to augment the functional properties to improve the dielectric and magnetoelectric properties by substitutions on Bi-site and/or Fe-site [8-14]. On the other hand, modification of either magnetic or dielectric properties of BFO has been reported through the divalent ion doping (i.e., Ca²⁺, Ba²⁺, Pb²⁺, and Sr²⁺) [15, 16]. Also structural changes at long range and micro/nano level have been imparted on the rhombohedral structure of BFO by divalent substitution for Bi. Mainly studies have revealed a weakening of the rhombohedral R3c structure and the transformation to the cubic Pm-3m structure while some studies do not come across any such structural change [17, 18]. Kundys et al has reported the magnetic field induced polarization ($P_r = 96 \mu\text{C}/\text{cm}^2$ at 10 T) for Bi_{0.75} Sr_{0.25} FeO_{3- δ} samples which is among the highest reported in either thin film or bulk forms of BFO based systems [19]. Such fascinating properties motivate to make choice of Sr compared to other divalent substituent. There are several synthesis methods like solid state synthesis, Pechini Method, sol gel technique, hydrothermal method, combustion synthesis being used by researchers. In our work opting combustion method technique is due to its simplicity, cost effectiveness and the broad applicability range. Also the combustion reaction is very fast (~ few seconds) that many defects are introduced into structure during it, which lowers required sintering temperatures and, hence, helps in obtaining nanomaterials [20].

Thus different results with regard to different functional properties have been reported in a number of studies for Sr substituted BFO. In this paper, attempts have been made to substitute the transition metal ion, Sr ion having ionic radius ~1.26 Å on Bi-site and thoroughly study the effect of Sr substitution on optical and dielectric properties of BSFO nanocomposite. The complex impedance spectroscopic data and AC conductivity studies have been analyzed to understand the electrical properties of these materials. However, to best of our knowledge, no thorough study has been reported on the dielectric properties and complex impedance analysis of the Sr doped bismuth ferrite so far.

2. EXPERIMENTAL DETAIL

2.1 Synthesis

Sr doped Bismuth Ferrite [Bi_{1-x}Sr_x FeO₃; x=0.1, 0.2, 0.3] nanoparticles have been prepared by a combustion method employing the use of metal nitrates and citric acid but without any solvent. Bi (III)

nitrate pentahydrate $[\text{Bi}(\text{NO}_3)_3 \cdot 5\text{H}_2\text{O}]$, Fe (III) nitrate nonahydrate $[\text{Fe}(\text{NO}_3)_3 \cdot 9\text{H}_2\text{O}]$, Sr (II) nitrate $[\text{Sr}(\text{NO}_3)_2]$ and citric acid ($\text{C}_6\text{H}_8\text{O}_7$) were procured from 'SD Fine-Chem limited' (SDFCL), Mumbai (India) with 99.9% purity have been used to prepare nanoparticles of $\text{Bi}_{1-x}\text{Sr}_x\text{FeO}_3$. These compounds were taken in stoichiometric ratios in a glass beaker and mixed with constant stirring while being heated at 80°C on a hot plate for about 25 minutes. Then, the mixture in the form of thick gel was heated at 150°C for combustion of the mixture. to form brown precursor which was grounded into powder using mortar and pestle. Finally the precursor powder was annealed in high purity alumina crucibles in air at 600°C for 2 hours and then slowly cooled down to room temperature. The crystallite size of BSFO ($\text{Bi}_{1-x}\text{Sr}_x\text{FeO}_3$) was found to be 49.42 nm for $x = 0.1$ and 44.93 nm for $x = 0.2$ and 0.3 along with traces of secondary phases in our earlier studies described elsewhere [21]. The samples were pressed into a pellet of 7 mm diameter and about 1 mm thickness by applying pressure $\sim 250\text{kg}/\text{cm}^2$ (with 5% PVA aqueous solution as a binder). Thereafter the pellets were sintered at 600°C for 2 hours and then polished to acquire smooth surface. The contacts for electrical measurements were made using silver paste on the flat surfaces of the sintered pellets.

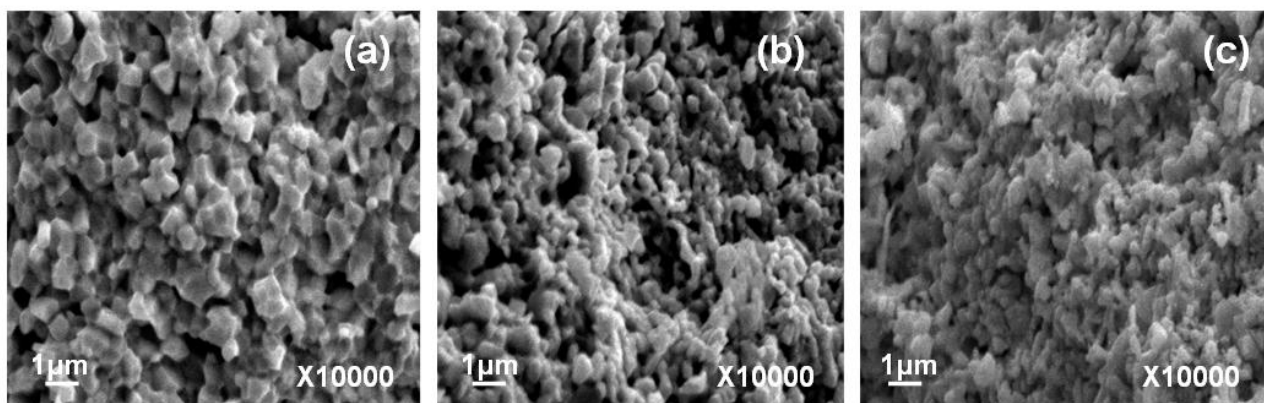
2.2 Characterizations

The optical properties of the samples were analyzed by using FTIR and UV-Vis spectrophotometer. Light absorption was measured using Shimadzu 2500 UV-vis spectrometer configured in diffused reflectance mode (DRS), using an integrating-sphere attachment over a spectral range of 290 to 800 nm. Scanning Electron Microscopy (SEM) and Energy Dispersive Spectroscopy (EDS) has been employed to study the structural morphology of the samples. The dielectric studies and complex impedance spectroscopic analysis were carried out as a function of frequency (20 Hz – 1 MHz) and temperature (300 K – 723 K) using a Impedance Analyzer (model- Wayn Kerr 6500B).

3. RESULTS AND DISCUSSION

3.1 Structural Analysis

Fig. 1 (a-c) shows the microstructure of the fractured surfaces of different BSFO samples.



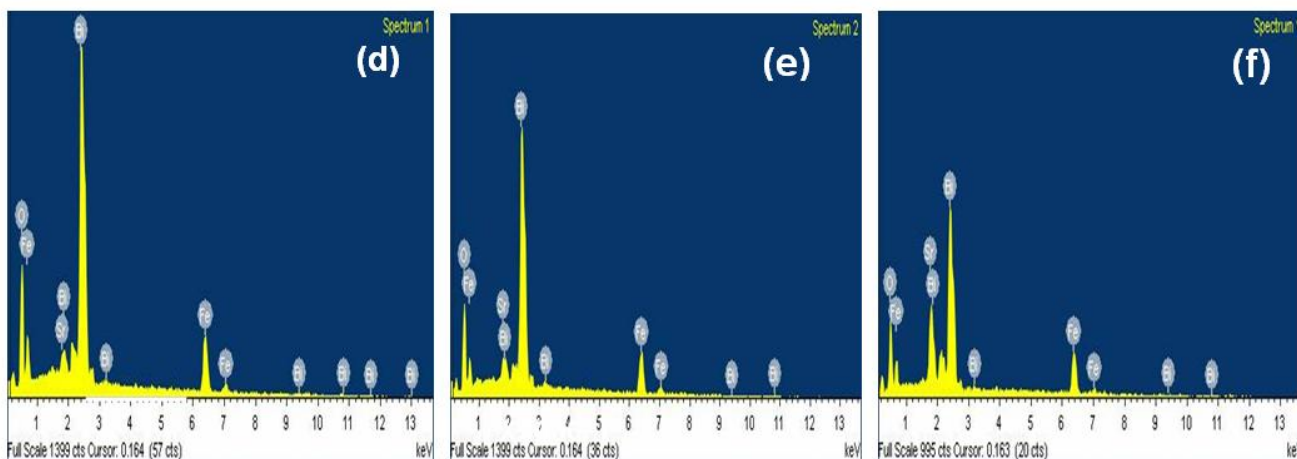


Figure 1. SEM (a-c) and EDS (d-f) of fractured samples of $\text{Bi}_{1-x}\text{Sr}_x\text{FeO}_3$ ($x = 0.1, 0.2, 0.3$)

These images revealed that with increased Sr concentration in BSFO samples, the grain size has found to be decreased. It might be due to Sr-doping that up to a certain level inhibits grain growth. The presence of secondary phase may also inhibit the grain growth. The chemical composition profile of the samples was determined using energy dispersive spectroscopy (EDS) as shown in Fig. 1(d-f). The EDS curves were taken at a number of selected positions of the samples and all have shown the expected presence of Bi, Sr, Fe and O.

3.2 Optical studies

Fourier transformed infrared (FTIR) spectra of Sr substituted samples were shown in Fig. 2.

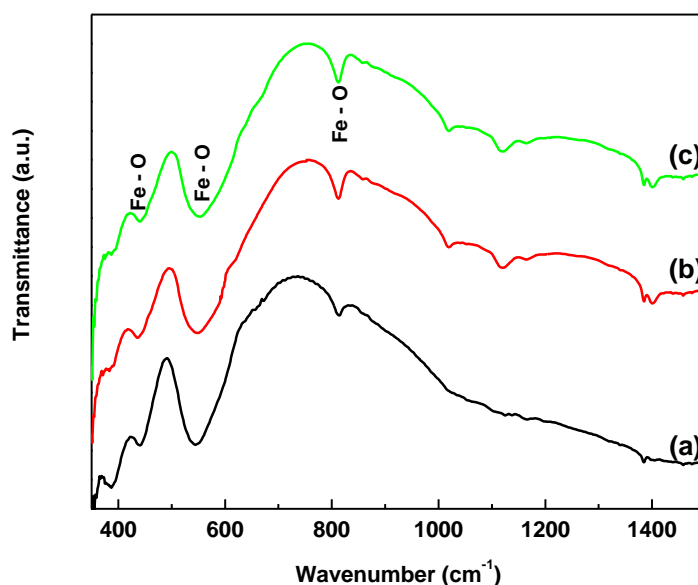


Figure 2. FTIR spectra of nanoparticles $\text{Bi}_{1-x}\text{Sr}_x\text{FeO}_3$ (a) $x=0.1$, (b) $x=0.2$, (c) $x=0.3$

Spectral analysis is performed in the scan range of $1500\text{--}375\text{ cm}^{-1}$. The characteristic vibration of the octahedral FeO_6 complex group which are assigned to Fe–O stretching and bending vibration are observed in the form of strong absorption peaks near 545 cm^{-1} and 440 cm^{-1} , respectively; implying the formation of BFO phase. Moreover, another Fe–O peak indicating the formation of a highly crystalline BFO phase was also observed at 810 cm^{-1} . These band positions are found to be in agreement with the characteristic infrared absorption bands of BFO [22]. The band around 1380 cm^{-1} arose due to the presence of trapped nitrates [23].

Fig 3(a) shows the room temperature UV–visible absorption spectra for $\text{Bi}_{1-x}\text{Sr}_x\text{FeO}_3$ ceramics with $x=0.1, 0.2, 0.3$ in the spectral ranges $1.0\text{--}3.5\text{ eV}$.

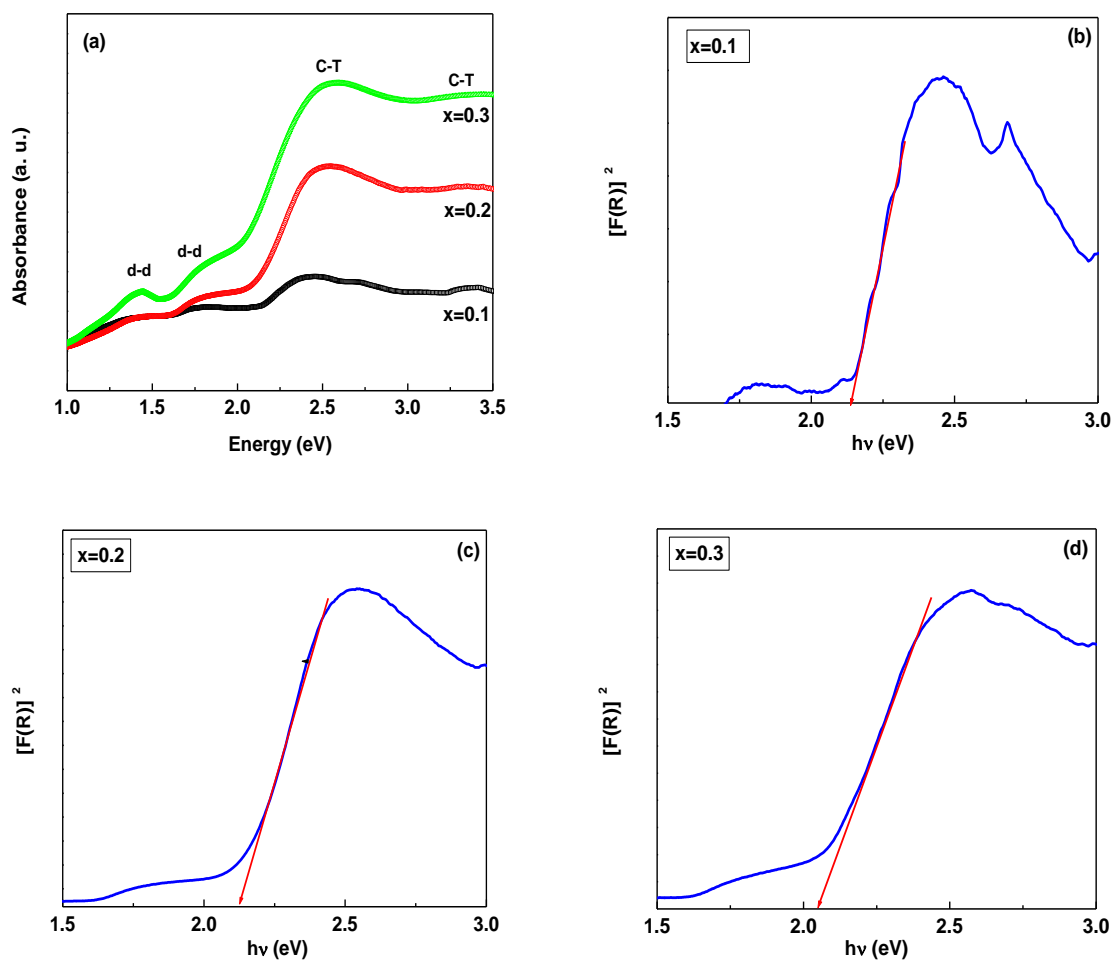


Figure 3. UV–vis diffuse reflectance spectra of various samples (a) $\text{Bi}_{1-x}\text{Sr}_x\text{FeO}_3$; $x=0.1, 0.2, 0.3$ and (b)–(d) is the square of Kubelka–Munk functions $F(R)$ versus photo energy

The two broad bands around 1.4 and 1.8 eV has been observed that corresponds to d–d transitions of Fe^{3+} ions as degenerate d orbital undergo splitting due interaction with ligand. These are theoretically forbidden excitations as reported in literature [24]; however, spin–orbit coupling becomes the reason of relaxation from the selection rule and so these show small intensity [24]. The absorption

steadily increases up to 2.5 eV and shows two broad bands pertaining to charge transfer (CT), one around 2.5 eV and another broad band around 3.2 eV. The CT band around 2.5 eV is attributed to $\text{Fe}_{13d}\text{-Fe}_{23d}$ inter-site electron transfer, whilst band at 3.3 eV is associated to interatomic O 2p–Fe 3d transitions [25].

Also a noticeable shift in d–d and charge transfer bands is observed with increase in Sr doping. The Sr substitution in BSFO samples results in chemical stress as the volume of unit cell increases (shown elsewhere) [21], which alter the surroundings of FeO_6 octahedron local environment and hence causes shift in transition bands.

Kubelka-Munk (K-M) method has been employed to convert UV-Vis diffuse reflectance spectra into absorption reading according to the [26]. The absorption spectrum of the samples was obtained from the diffuse reflection spectra using Kubelka-Munk function:

$$F(R) = (1-R^2)/2R$$

Where, R is diffuse reflectance. The absorption spectra of the prepared $\text{Bi}_{1-x}\text{Sr}_x\text{FeO}_3$ samples transformed from the DRS spectra according to the Kubelka–Munk (K–M) theory is shown in Fig.3. The $[F(R)]^2-(h\nu)$ curves for all samples reveal a good fit with the direct band gap process and energy band gap is determined by extrapolating the linear portion of this curve to zero. The optical band gap was calculated to be 2.14, 2.12, 2.05 eV for $x=0.1, 0.2$ & 0.3 samples respectively. Thus it concludes that the orientation of oxygen octahedral and presence of defects in the samples might be attributed to the decrease of the band gap and which has been the main cause in the enhancement of magnetization depicted elsewhere [21].

3.3 Dielectric Studies:

Frequency dependence of the dielectric constant (ϵ) of the samples is measured at RT (Fig. 4.).

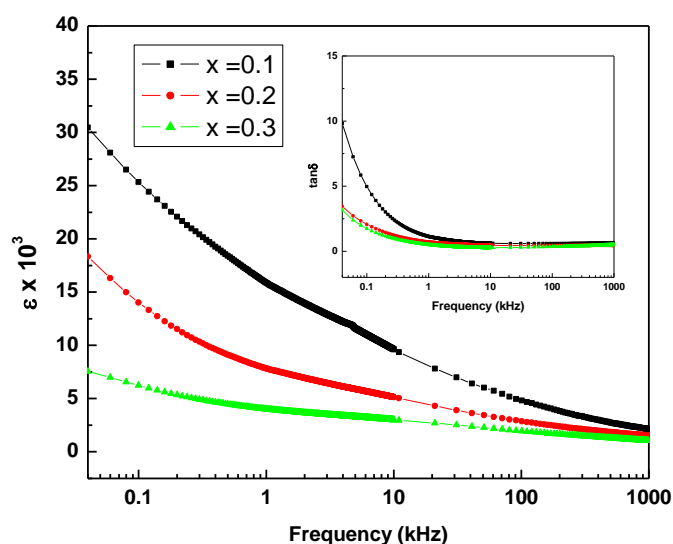


Figure 4. Room temperature frequency dependence of ϵ and $\tan \delta$ (inset) of $\text{Bi}_{1-x}\text{Sr}_x\text{FeO}_3$ ($x = 0.1, 0.2, 0.3$) samples

It is observed that with the increase in frequency, the value of dielectric constant decreases up to 100 kHz, thereafter it becomes almost constant for all the samples. The presence of all types of polarizations (dipolar, ionic, atomic and interface) may be primarily responsible for this type of trend at very low frequency for the samples. The value of ϵ_r increases with increase in space charge polarization, which in turn may be due to a large concentration of defects [27]. But on increasing frequency, some of the polarizations slowly vanish except ionic and electronic polarization, which results in rapid decrease in dielectric constant. The value of dielectric constant also relies on some other features such as void, grain boundaries and dipolar interaction [28]. Inset Fig. 4. shows the variation of $\tan \delta$ with frequency for $\text{Bi}_{1-x}\text{Sr}_x\text{FeO}_3$. The value of $\tan \delta$ is high in the low-frequency region in these compounds, and shows a significant decrease with rise in frequency [29]. The suppression of dipolar contribution towards the polarization at high frequencies owes this decreased value of $\tan \delta$ [30].

Fig.5. shows the ϵ and $\tan \delta$ (inset Fig.5) versus temperature plots of all the samples at a frequency 10 kHz.

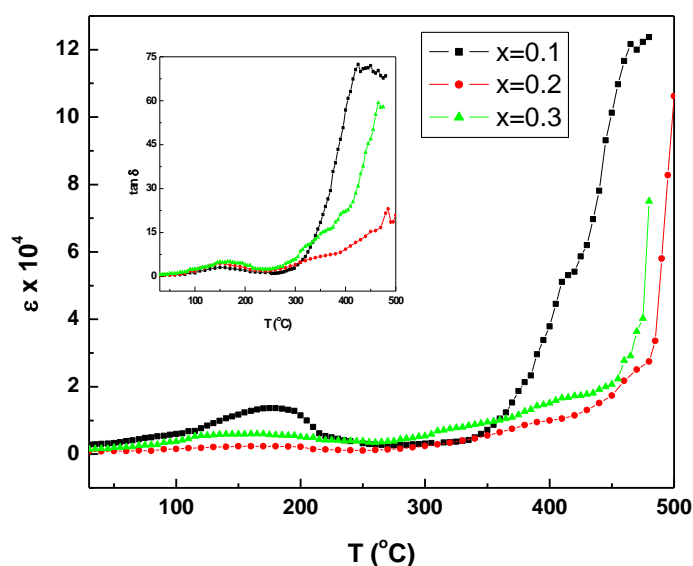


Figure 5. Temperature dependent plots of ϵ and $\tan \delta$ (inset) for for the samples $\text{Bi}_{1-x}\text{Sr}_x\text{FeO}_3$ ($x = 0.1, 0.2, 0.3$) at 10 kHz

Dielectric constant versus temperature plot of BSFO ($x = 0.1$ to $x=0.3$) exhibited one anomaly peak at around 170°C . Catalan et.al also addressed anomaly around 185°C , whose origin needed further investigations [7]. But around 350°C , which is close to the magnetic transition temperature (370°C) of BFO, ϵ of all the samples increases sharply [13]. Since magnetic and electric orderings are coupled in these materials, a change in magnetic ordering clearly affects the ϵ value. The anomaly around magnetic transition temperature (370°C) of BFO is not observed, this may be due to high conductivity and space-charge effect of the BSFO samples at high temperatures. As thermally activated process dominates in this temperature range, which enhances the loss tangent to very high value [31].

The dielectric constant ϵ and $\tan \delta$ for BSFO sample was found to decrease with increase in Sr doping and is maximum for BSFO ($x = 0.1$). The decrease in the dielectric values may be attributed to resultant effect of the two phenomenons. One is the expected introduction of more oxygen vacancies due to charge compensation with substitution of the Sr ions in BFO which in turn increases the probability of the hopping conduction mechanism. The other reason might be due to the substitution of higher radii Sr ion and presence of traces of secondary phase which gives rise to reduced grain sizes (increased grain boundaries) and in-homogeneity (as shown in SEM), which in turn poses hindrances to the charge movement. It clearly suggests that Sr-substitution in bismuth ferrite have a considerable effect on dielectric properties of BSFO.

3.4 Complex Impedance Spectroscopy

Complex impedance spectroscopy is a comparatively effective method of explaining many of the electrical properties of materials [13]. It provides an important tool to establish relationship between microstructures and the electrical properties of polycrystalline material. This technique involves measurement of output response across the pellet sample on applying an ac signal. Most of the real ceramics contain grains and grain boundary regions, which exhibits very different physical properties. The analysis of the complex impedance data can preferably be done by using an equivalent circuit consisting of two parallel combinations of R (resistance) and C (capacitance) components in a circuit.

Electrical AC data may be presented in any of the four interrelated formalism: relative permittivity $\epsilon^* = \epsilon' - j \epsilon''$; impedance $Z^* = Z' + j Z'' = 1 / j\omega C_o \epsilon^*$; electric modulus $M^* = M' + jM'' = 1 / \epsilon^*$; admittance $Y^* = Y' + jY'' = j\omega C_o \epsilon^*$; and $\tan \delta = \epsilon'' / \epsilon' = M'' / M' = Z'' / Z' = Y'' / Y'$, where $f =$ frequency; $\omega = 2\pi f$ is the angular frequency; $C_o = \epsilon_o A/t$ is the geometrical capacitance; $j = \sqrt{-1}$; ϵ_o is the permittivity of vacuum (8.854×10^{-12} F/m); t and A are the thickness and area of the pellet; and δ is complementary ($90 - \theta$) to the phase angle (θ).

3.4.1 Impedance Studies

Fig. 6 shows the variation of real part (Z') and imaginary part (Z'') [inset Fig.6.] of impedance of BSFO with frequency at room temperature.

The magnitude of Z' was found to decrease monotonically with increase in frequency, and reached a constant value in the high frequency region. This type of tendency was revealed by all BSFO samples without any anomalous behaviour. The plateau region of the graph also point to the presence of a relaxation process in the material.

The loss spectrum (Z'') has some important features: (i) the appearance of a peak in the loss spectrum $\max Z''$ (ii) typical peak broadening. The appearance of peaks suggested the existence of relaxation properties and these peaks emerge when the hopping frequency of localized electrons becomes of the order of the frequency of applied field. The occurrence of relaxation peaks could be ascribed to the presence of immobile species/electrons at low temperatures and defect/vacancies at

high temperature. The asymmetric peak broadening suggests a spread of the relaxation time [12]. The peak height in Z'' against frequency plot is proportional to the resistance of that process, while the peak height in M'' against frequency plot is inversely proportional to the capacitance.

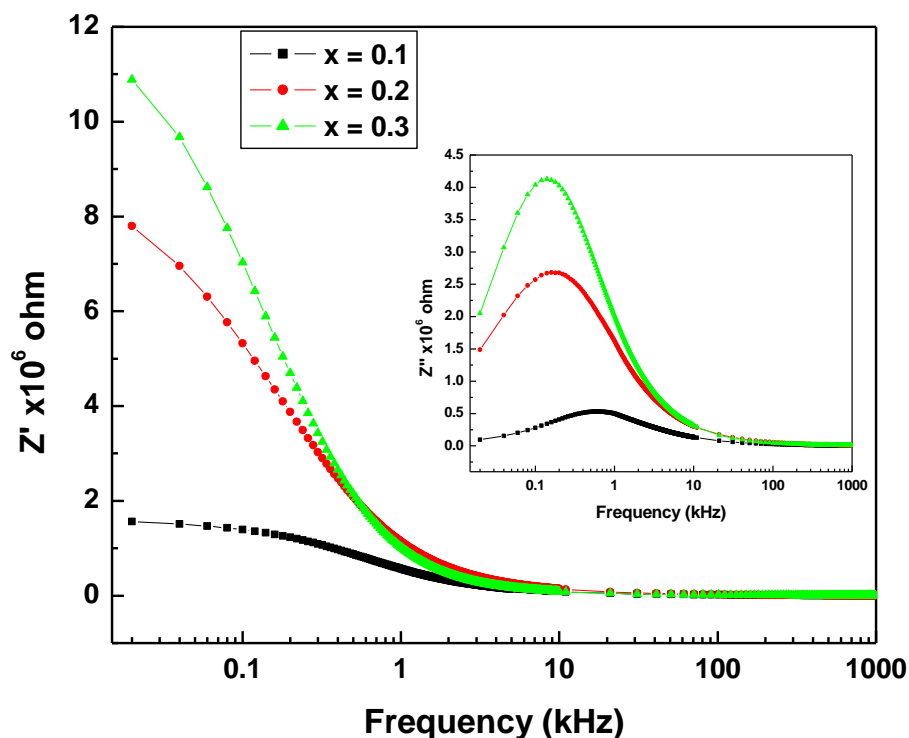


Figure 6. Room temperature frequency dependence of Z' and Z'' (inset) of $\text{Bi}_{1-x}\text{Sr}_x\text{FeO}_3$ samples

The values of Z' and Z'' were observed to merge above 10 kHz. The conductivity across grain boundaries and the increased hopping of charge carriers between the localized ions at high frequencies might be the underlying factors for this trend. Moreover, the magnitude of Z' and Z'' gradually increased with the Sr concentration. This indicated the decrease in conduction path due to hindrance posed by grain boundaries.

The Nyquist Plot i.e. Z'' vs Z' of BFSO is displayed in fig. 7.

The complex impedance plots of all samples consist of depressed semicircular arcs indicates the possibility of having more than one relaxation in the sample. Also the centre of arc lies below the real axis that shows the presence of non-Debye type of relaxation phenomenon in the samples.

The intercept of the semicircle on the real axis gives the resistance of grain (R_b) and grain boundary (R_{gb}) of the corresponding component contributing towards the impedance of the sample. The observed increase in size of semicircular arcs with increase in Sr doping is attributed to the increase in resistance of corresponding components in the samples which is corroborated by SEM of samples as decrease in grain size increases grain boundaries which in turn poses more resistance. Since the size of the semicircles emerging in the impedance plot depends on the resistive responses of the

components. It is difficult to resolve the responses coming from the grain and grain boundary if the difference in their resistances is large [13]. Further understanding of different relaxations could be achieved by electric modulus studies that depend on the capacitance.

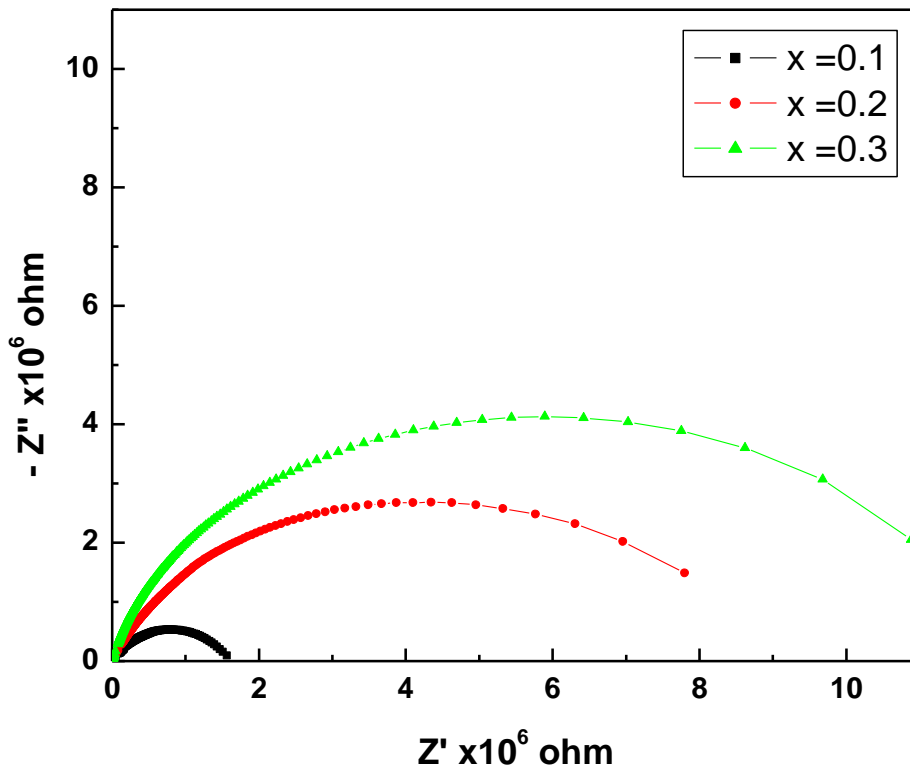


Figure 7. Complex impedance spectra (Z' vs Z'') of $\text{Bi}_{1-x}\text{Sr}_x\text{FeO}_3$ samples at room temperature

3.4.2 Electric modulus studies

The relaxation properties of ionic conductors and polycrystalline ceramics are usually described using dielectric modulus formalism [32]. Modulus spectroscopy plots are predominantly useful tools for segregating spectral components of materials with similar resistances but having different capacitances. The other advantage of representing electrical relaxation in modulus formalism is that the electrode polarization effects are suppressed in this representation. Due to the above reasons, complex electric modulus formalism has been preferred. The imaginary part of electrical modulus is indicative of energy loss in the structure under electrical field. For the dielectric relaxation, studies have been carried out in the complex modulus M^* formalism and is calculated as [33]

$$M^*(f) = 1/\epsilon^*(f) = M'(f) + i M''(f)$$

Variation of real (M') and imaginary (M'') parts of the electric modulus as function of frequency at room temperatures are shown in Fig. 8 and its inset.

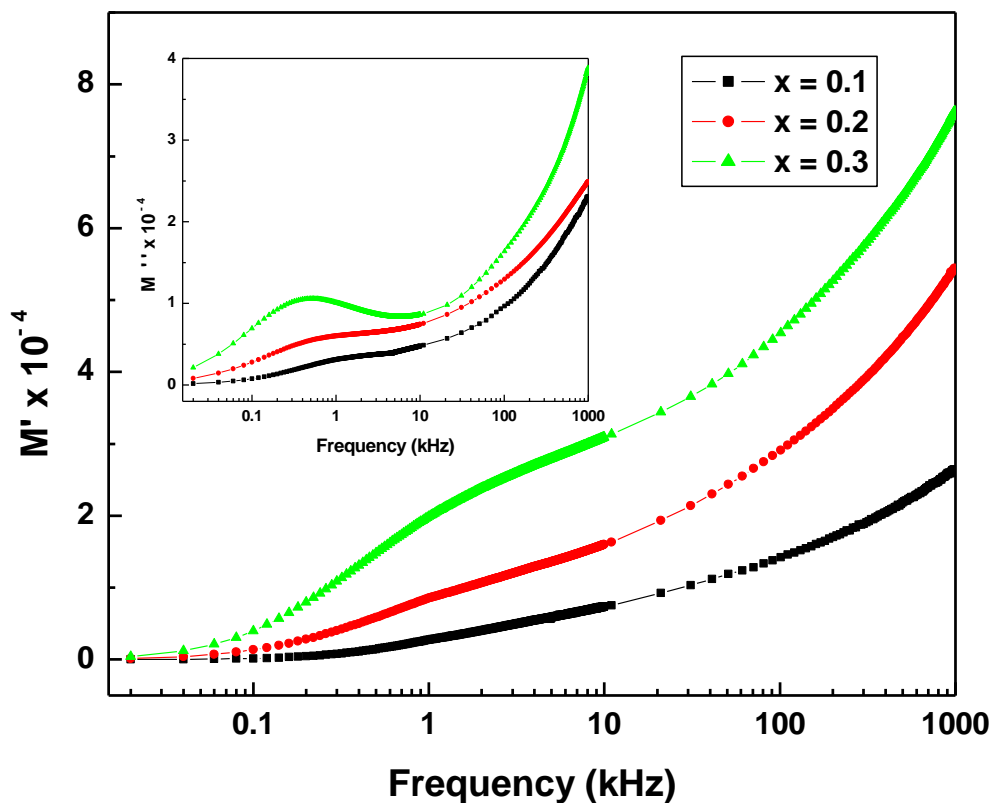


Figure 8. Room temperature frequency dependence of M' and M'' (inset) of $\text{Bi}_{1-x}\text{Sr}_x\text{FeO}_3$ samples

M' is found to be very low at lower frequencies and shows an increasing trend with the increase in frequency. It shows continuous dispersion on increasing frequency which may be due to an induced electric field driven short range mobility of charge carriers. The value of M' increases with frequency and the dispersion shifts to lower frequencies as Sr doping increases.

The dependences of M'' on frequency (inset Fig. 8) reveal the emergence of two asymmetric modulus peaks at low as well as at high frequencies. The observed asymmetry in peak broadening indicates the spread of relaxation time with different time constant which supports the non-Debye type of relaxation in the materials. The low frequency peak suggests that ions can move over long distances by hopping from one site to the neighbouring site whereas high frequency peak supports the confinement of ions in their potential well and can execute only localized motion [34]. With the decrease in grain size, the grain boundary volume increases which in turn increases the number of dipoles in the grain boundary in a nano crystalline material. Consequently, the interaction among the dipoles within the grain boundary increases which slows down the dipole relaxation, reducing the relaxation frequency [35] which might be the reason of shifting of relaxation peak position towards lower frequencies with the increase in Sr content. It is observed that M' and M'' corresponding to the peaks is maximum in case of BSFO with $x = 0.03$.

The complex modulus spectrum (i.e. M' vs. M'' spectrum) of BFSO at room temperature is shown in Fig.9.

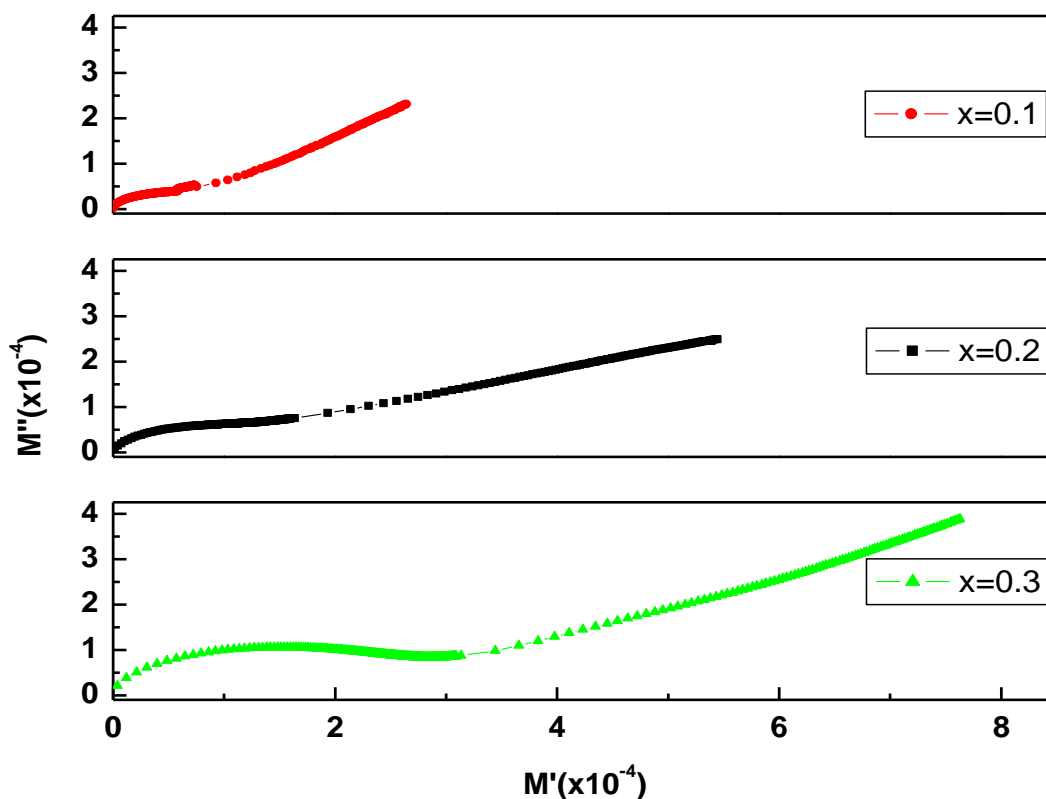


Figure 9. Complex modulus spectra (M' vs M'') of $\text{Bi}_{1-x}\text{Sr}_x\text{FeO}_3$ samples at room temperature

The semi-circular arcs are observed in the form of two semicircular arcs (or tendency) which indicates the presence of both grain and grain boundary contributions in the BSFO nanocomposites. Their centres appear to lie below the real M' -axis so it indicates spread of relaxation with different (mean) time constant and hence supports the non-Debye type of relaxation in the materials [36]. It is clear that the modulus plane shows two semicircles (tending), the intercept of the first (smallest) semicircle with the real axis designates the total capacitance contributed by the grain boundary, while the intercept of the second semicircle to that contributed by the grain. Intercepts of these semicircles on real axis appear to shift towards higher values of M' with the increase in Sr content. It indicates decrease in capacitance with the increase in Sr content as intercept on M' axis is inversely proportional to capacitance of corresponding contribution. The capacitance in turn is inversely proportional to the resistance. Thus the increase in resistance of grain and grain boundary contributions is observed with increase in Sr content which is in correspondence with impedance studies.

3.5 Electrical AC Conductivity Analysis

The frequency dependence of conductivity (Fig.10) shows two distinct regime, within the measured frequency window limit, i) the plateau and ii) dispersion.

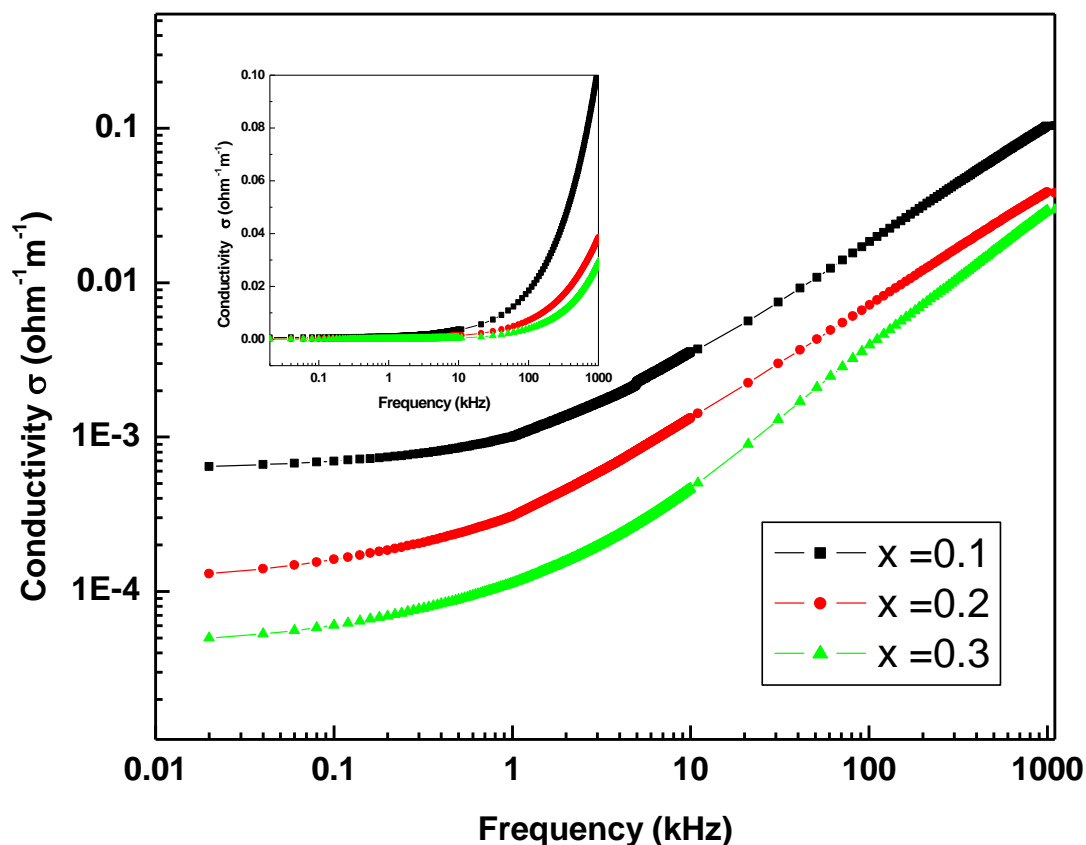


Figure 10. Room temperature frequency dependence of AC electrical conductivity (inset) of $\text{Bi}_{1-x}\text{Sr}_x\text{FeO}_3$ samples and in log scale

The plateau corresponds to the frequency independent conductivity σ_{dc} . The σ_{dc} value is obtained by extrapolating the conductivity value to the lower frequency [37]. The increase in frequency of the applied field enhances the charge carrier's jumps between the localized states, which results in increase of conductivity. The nature of the conductivity curve is in resemblance to the reported systems of $\text{Sm}_x\text{Bi}_{1-x}\text{FeO}_3$, $\text{Bi}_{0.8}\text{Sr}_{0.2}\text{Fe}_{1-x}\text{Nb}_x\text{O}_3$, Ba doped BiFeO_3 , Gd-doped BiFeO_3 [37–40].

The variations of ac conductivity (σ_{ac}) for all the doped samples as a function of the reciprocal of the absolute temperature at 10 kHz were shown in Fig.11. It is clearly seen that the substitution alters the nature of the conductivity curve as a function of temperature especially at higher temperatures [Inset Fig.11]. A weak dependence of conductivity in low temperature region shows a short range of hopping of defects. Different activation energy is observed in different temperature regions of the ac conductivity curve as shown in Fig.11 The trend of region I, II and III is very same and getting an effective shape on Sr substitution. The value of activation energy of the samples in region I varies from 0.75 to 2.15 eV, and in region III varies from 0.37 to 0.51eV which indicates the contribution of long-range motion of oxygen vacancy in the conduction mechanism [14], in region III, the value indicates that impurity conduction along with short-range hopping motion of oxygen vacancy

might prevail in this temperature region. In samples $x = 0.1, 0.2$ and 0.3 , the region II shows a decreasing trend and it might be due to the alteration of carrier concentration of charge carriers [39].

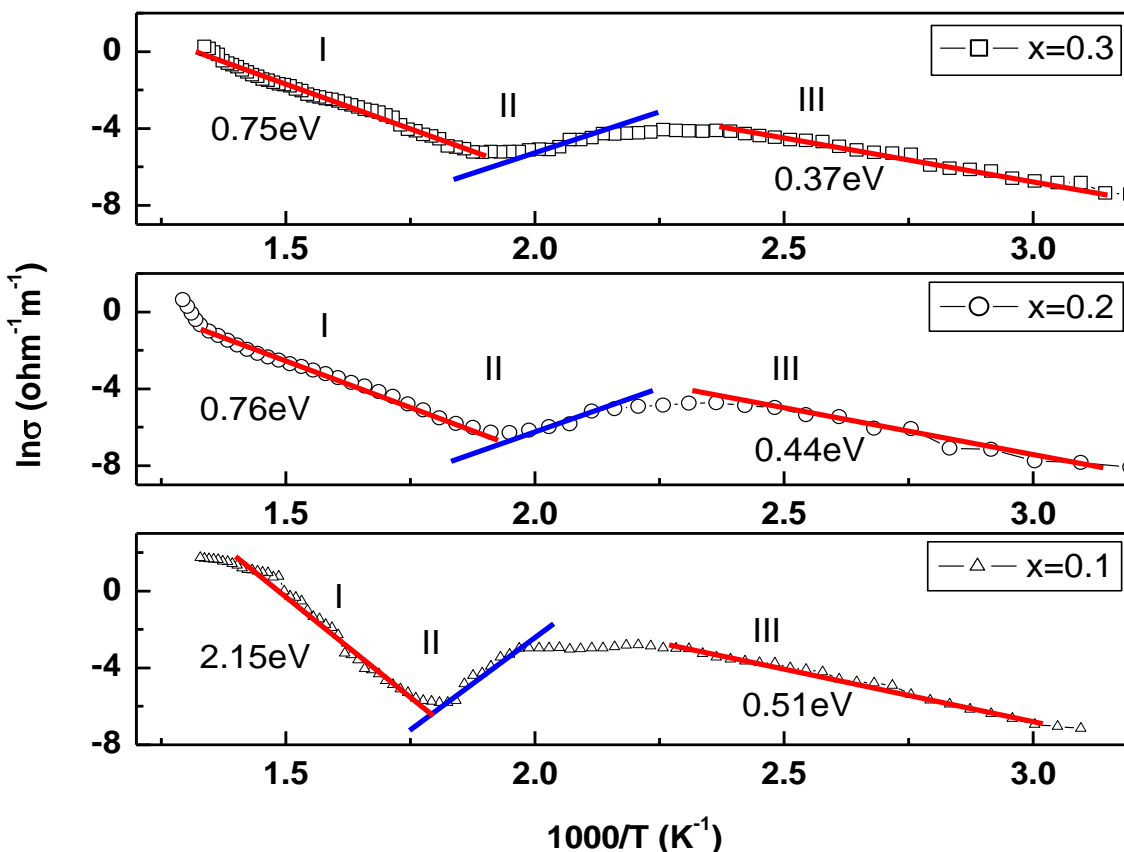


Figure 11. AC conductivity ($\ln \sigma$) as a function of the reciprocal of the absolute temperature $\text{Bi}_{1-x}\text{Sr}_x\text{FeO}_3$

However, it is clear that conductivities of samples having different doping levels depend on the amounts of defects and impurity phases. It seems that even up to high temperatures BSFO is not dominated by the intrinsic conductivity that would result from the optical gap, but merely due to defect and impurity contributions. But smaller amount of oxygen vacancies and secondary phase might be the reason for BSFO ($x=0.1$) where activation energy (2.15 eV) from conductivity studies well corroborated by the optical band gap as obtained from UV-vis studies.

4. CONCLUSIONS

In summary, we have synthesized Sr doped bismuth ferrite (BSFO) samples using combustion method. The Fourier transformed Infrared (FTIR) and Ultra Violet Visible (UV-Vis) spectra at room temperature show a change in spectral behavior on substitution for all the samples. The optical band

gap was found to decrease with increasing Sr concentration due to the variation in local FeO₆ environment. The complex impedance and modulus spectroscopy analyses showed the dielectric relaxation in the material to be of non-Debye type. On Sr addition the dielectric constant shows a decrease which is corroborated to the change in the grain size and the growth of oxygen vacancies. The perceptible change in the dielectric constant near Neel temperature manifested the magnetoelectric coupling between electric and magnetic orders. The impedance studies exhibit the presence of grain (bulk) and grain boundary effects in the BSFO samples. Measurements of ac electric properties illustrate a remarkable difference in the ac conductivity at different temperatures on Sr substitution and the strong temperature dependence of conductivity in the high temperature region attributes to hopping due to oxygen defects. Furthermore, this study envisaged negative temperature coefficient of resistance behaviour of the samples. The room temperature ferromagnetism along with tuneable optical band gap in visible region of BSFO nanoparticles may find potential applications in photo catalytic activity and optoelectronic devices.

ACKNOWLEDGEMENTS

The authors acknowledge I. K. Gujral Punjab Technical University, Kapurthala for providing research facilities. The authors are also grateful to Sophisticated Analytical Instrumentation Facility, Punjab University Chandigarh for providing X-Ray Diffraction facility. The cooperation and help rendered in the research work by the staff of Department of Applied Physics, Giani Zail Singh Campus College of Engineering and Technology Bathinda is also acknowledged. In addition, the first author acknowledges University Grant Commission (UGC), New Delhi for providing teacher fellowship and the parent organization Punjabi University Patiala, Punjab (India) for granting study leave to pursue research work.

References

1. G. Catalan, J. F. Scott, *Adv. Mater.*, 21 (2009) 2463
2. M. Fiebig, *J. Phys. D: Appl. Phys.*, 38 (2005) 123
3. C. Ederer, N. A. Spaldin, *Phys. Rev. B.*, 71 (2005) 060401
4. F. Kubel, H. Schmid, *Acta Crystallographica B*, 46 (1990) 698
5. J. Wang, J.B. Neaton, H. Zheng, V. Nagarajan, S.B. Ogale, B. Liu, D. Viehland, V. Vaithyanathan, D.G. Schlom, U.V. Waghmare, N.A. Spaldin, K.M. Rabe, M. Wuttig, R. Ramesh, *Science*, 299 (2003) 1719
6. T. Kimura, S. Kawamoto, I. Yamada, M. Azuma, M. Takano, and Y. Tokura, *Phys. Rev. B.*, 67 (2003) 180401
7. G. Catalan, J. F. Scott, *Adv. Mater.*, 21 (2009) 2463
8. B. Bhushan, A. Basumallick, N.Y. Vasanthacharya, S. Kumar, D. Das, *Solid State Sciences*, 12 (2010) 1063
9. R. Mazumder, A. Sen, *J. Alloys Compd.*, 475 (2009) 577
10. J.B. Li, G. H. Rao, J. K. Liang, Y. H. Liu, J. Luo and J. R. Chen, *Appl. Phys. Lett.*, 90 (2007) 16251
11. Y. Li, W. Cao, J. Yuan, D. Wang and M. Cao, *J. Mater. Chem. C.*, 3 (2015) 9276
12. A. Kumar, K.L. Yadav, *Physica B*, 405 (2010) 4650
13. R. Das, T. Sarkar and K. Mandal, *J. Phys. D: Appl. Phys.*, 45 (2012) 455002
14. P. Pandit, S. Satapathy, P. K. Gupta, *Physica B: Condensed Matter*, 406 (2011) 2669

15. S. Hussain , S.K. Hasanain , G. Hassnain Jaffari , Naveed Zafar Ali , M. Siddique , S. Ismat Shah, *Journal of Alloys and Compounds*, 622 (2015) 8
16. V.A. Khomchenko, D.A. Kiselev, J.M. Vieira, L. Jian, A.L. Kholkin, A.M.L. Lopes, Y.G. Pogorelov, J.P. Araujo, M. Maglione, *J. Appl. Phys.*, 103 (2008) 024105
17. S.K. Mandal, T. Rakshit, S.K. Ray, S.K. Mishra, P.S. Krishna, A. Chandra, *J. Phys.: Condens. Matter.*, 25 (2013) 55303
18. E. Pachoud, Y. Breard, C. Martin, A. Maignan, A.M. Abakumov, E. Suard, R.I. Smith, M.R. Suchomel, *Solid State Commun.*, 152 (2012) 33
19. B. Kundys, A. Maignan, C. Martin, N. Nguyen, C. Simon, *Appl. Phys. Lett.*, 92 (2008) 112905
20. K.C. Patil, M.S. Hegde, T. Rattan, S. Aruna, *Chemistry of Nanocrystalline Oxide Materials*, World Scientific Publishing Co. Pte. Ltd., Singapore (2008) ISBN: 978-981-279-314-0
21. B. Kaur, L. Singh, V. Annapu Reddy, D.Y. Jeong, N Dabra and J. S. Hundal, *Structural, magnetic and electric properties of Sr doped BiFeO₃ nanoparticles synthesized by citrate combustion method* (communicated)
22. V. A. Reddy, N. P. Pathak and R. Nath, *Phys. Scr.*, 86 (2012) 065701
23. C. Chao, C. Jinrong, Y. Shengwen, C. Lingjuan, M. Zhongyan, *J Cryst Growth.*, 291 (2006) 135
24. T. Durga Rao, T. Karthik, S. Asthana, *J. Rare Earths*, 31(2013) 370
25. R.V. Pisarev, A.S. Moskvina, A.M. Kalashinkova, T. Rasing, *Phys. Rev. B.*, 79 (2009) 235128
26. P. Kubelka, F. Munk, *Z. Tech. Phys.*, (Leipzig) 12 (1931) 593
27. S. Pattanayak, R.N.P. Choudhary, P. R. Das, *J. Mater. Sci.: Mater. Electron.*, 24 (2013) 2767
28. B.K. Barick, K.K. Mishra, A.K. Arora, R.N.P. Choudhary, Dillip K. Pradhan, *J. Phys. D: Appl. Phys.*, 44 (2011) 355402
29. R.N.P. Choudhary, Dillip K. Pradhan, C.M. Tirado, G.E. Bonilla, R.S. Katiyar, *J. Mater. Sci.*, 42 (2007) 7423
30. F. Yan, M. On Lie, L. Lu, *J. Phys. Chem. C.*, 114 (2010) 6994
31. S. N. Tripathy , B.G. Mishra , M. M. Shirolkar , S. Sen , S. R. Das , D. B. Janesn, D. K. Pradhan, *Materials Chemistry and Physics*, 141 (2013) 423
32. J. Liu, C.G. Duan, W.G. Yin, W.N. Mei, R.W. Smith, J.R. Hardy, *J. Chem. Phys.*, 119 (2003) 2812
33. F. Gheorghiu , M. Calugaru , A. Ianculescu , V. Musteata , L. Mitoseriu, *Solid State Sciences.*, 1 23 (2013) 79
34. J.S. Kim, *J. Phys. Soc. Jpn.*, 70 (2001) 3129
35. T. Prakash, K. Padma Prasad, R. Kavitha, S. Ramasamy, B. S. Murty, *J. Appl. Phys.*, 102 (2007) 104104
36. R. Ranjan, N. Kumar, B. Behera and R.N.P. Choudhary, *Adv. Mat. Lett.*, 5 (2014) 138
37. W.K. Lee, B.S. Lim, J.F. Liu, A.S. Nowick, *Solid State Ionics*, 53-56 (1992) 831
38. Reetu, A. Agarwal, S. Sanghi, N. Ahlawat, Monica, *J. Appl. Phys.*, 111 (2012) 113917
39. A. Paul Blessington Selvadurai, V. Pazhanivelu, R. Murugaraj, *J Supercond Nov Magn.*, 27 (2014) 839
40. S. Pattanayak, B.N. Parida, P.R. Das, R.N.P. Choudhary, *Appl. Phys. A.*, 112 (2012) 387